Am J Physiol Endocrinol Metab 312: E150–E160, 2017.
First published December 13, 2016; doi:10.1152/ajpendo.00216.2016.

RESEARCH ARTICLE

Myostatin propeptide mutation of the hypermuscular *Compact* mice decreases the formation of myostatin and improves insulin sensitivity

Tamas Kocsis,[1] Gyorgy Trencsenyi,[2] Kitti Szabo,[1] Julia Aliz Baan,[1] Geza Muller,[1] Luca Mendler,[1] Ildiko Garai,[2] Hans Reinauer,[3] Ferenc Deak,[4] Laszlo Dux,[1] and Aniko Keller-Pinter[1]

[1]*Department of Biochemistry, Faculty of Medicine, University of Szeged, Szeged, Hungary;* [2]*Scanomed, Debrecen, Hungary;* [3]*INSTAND, Dusseldorf, Germany; and* [4]*Institute of Genetics, Biological Research Centre, Hungarian Academy of Sciences, Szeged, Hungary*

Submitted 8 June 2016; accepted in final form 30 November 2016

Kocsis T, Trencsenyi G, Szabo K, Baan JA, Muller G, Mendler L, Garai I, Reinauer H, Deak F, Dux L, Keller-Pinter A. Myostatin propeptide mutation of the hypermuscular *Compact* mice decreases the formation of myostatin and improves insulin sensitivity. *Am J Physiol Endocrinol Metab* 312: E150–E160, 2017. First published December 13, 2016; doi:10.1152/ajpendo.00216.2016.—The TGFβ family member myostatin (growth/differentiation factor-8) is a negative regulator of skeletal muscle growth. The hypermuscular *Compact* mice carry the 12-bp *Mstn(Cmpt-dl1Abc)* deletion in the sequence encoding the propeptide region of the precursor promyostatin, and additional modifier genes of the *Compact* genetic background contribute to determine the full expression of the phenotype. In this study, by using mice strains carrying mutant or wild-type myostatin alleles with the *Compact* genetic background and nonmutant myostatin with the wild-type background, we studied separately the effect of the *Mstn(Cmpt-dl1Abc)* mutation or the *Compact* genetic background on morphology, metabolism, and signaling. We show that both the *Compact* myostatin mutation and *Compact* genetic background account for determination of skeletal muscle size. Despite the increased musculature of *Compact*s, the absolute size of heart and kidney is not influenced by myostatin mutation; however, the *Compact* genetic background increases them. Both *Compact* myostatin and genetic background exhibit systemic metabolic effects. The *Compact* mutation decreases adiposity and improves whole body glucose uptake, insulin sensitivity, and ^{18}FDG uptake of skeletal muscle and white adipose tissue, whereas the *Compact* genetic background has the opposite effect. Importantly, the mutation does not prevent the formation of mature myostatin; however, a decrease in myostatin level was observed, leading to altered activation of Smad2, Smad1/5/8, and Akt, and an increased level of p-AS160, a Rab-GTPase-activating protein responsible for GLUT4 translocation. Based on our analysis, the *Compact* genetic background strengthens the effect of myostatin mutation on muscle mass, but those can compensate for each other when systemic metabolic effects are compared.

myostatin; *Compact* mice; skeletal muscle; insulin resistance; 2-deoxy-2-[^{18}F]fluoro-D-glucose

MYOSTATIN [growth/differentiation factor-8 (GDF-8)] is a member of the TGFβ superfamily and is expressed predominantly in skeletal muscle (31). Myostatin is synthesized as a precursor protein, promyostatin, which undergoes dimerization and proteolytic processing; promyostatin dimer is cleaved by furin proteases to NH_2-terminal propeptide fragments and COOH-terminal disulfide-linked myostatin dimer (24). However, the propeptides can still associate with myostatin dimer via noncovalent bonds to form a latent complex that sequesters functional myostatin by preventing its binding to the receptor (24, 45). Myostatin acts through activin type IIB receptor (ActRIIB) (24), and the signaling involves Smad2/3 transcription factors (23, 57); furthermore, it influences the phosphatidylinositol 3-kinase (PI3K)/Akt pathway, which is the key regulator of the anabolic and catabolic responses in skeletal muscle (53).

Myostatin regulates the proliferation and differentiation of myoblasts (23, 46); moreover, it also controls the activation and proliferation of satellite cells, the stem cells of skeletal muscle (29). Homozygous disruption of the myostatin gene (31), administration of myostatin propeptide (25), or naturally occurring myostatin gene mutations, e.g., in humans (38), mouse (42), cattle (20), or sheep (10), result in widespread increase of skeletal muscle mass ("double-muscled" phenotype). However, the effect of myostatin is not restricted to skeletal muscle. Beside the autocrine and paracrine effects, it can serve as an endocrine factor. Myostatin was reported to influence the synthesis and secretion of IGF-1 (insulin-like growth factor-1) in the liver, thereby regulating the amount of circulating IGF-1 (51).

Several studies suggest that loss of myostatin or reduction in active myostatin levels leads to increased insulin sensitivity. Myostatin-null mice have increased muscle mass and reduced body fat (14, 26, 32) and exhibit increased insulin sensitivity (14), which depends on AMP-activated protein kinase (55). Transgenic expression of myostatin propeptide prevents diet-induced obesity and insulin resistance (56), and the overexpression of follistatin-like 3, an inhibitor of members of the TGFβ family (6), or inhibition of myostatin by dominant-negative myostatin receptor (13) improves insulin sensitivity. Furthermore, increased serum and muscle myostatin levels were shown in insulin-resistant human individuals (17).

The naturally occurring *Compact* mutation of the myostatin gene arose in a selection program on protein amount and hypermuscularity conducted at the Technical University of Berlin (7, 8). Genetic analysis of the Hungarian subpopulation of the hypermuscular *Compact* mice identified a 12-bp deletion, denoted *Mstn(Cmpt-dl1Abc)*, in the propeptide of the promyostatin (42). The biologically active growth factor do-

Address for reprint requests and other correspondence: A. Keller-Pinter, Dept. of Biochemistry, Faculty of Medicine, University of Szeged, Dom square 9, H-6720 Szeged, Hungary (e-mail: keller.aniko@med.u-szeged.hu).

main of myostatin is unaffected by *Compact* mutation; therefore, the loss of myostatin activity cannot be explained by disruption of the growth factor bioactive domain. However, the mutation can lead to misfolding or defect in secretion and mistargeting of mature myostatin (42). Additional modifier genes should be present to determine the full expression of the *Compact* phenotype; however, these modifier genes of the special *Compact* genetic background have not yet been identified (47, 48). Furthermore, the molecular consequences of *Compact* myostatin mutation, which can regulate muscle size and metabolism, have not been examined. In this study, by using a congenic wild-type mice strain with wild-type myostatin and *Compact* genetic background, we could separately study the effect of *Compact* myostatin mutation and genetic background on morphology, metabolism, and signaling. The *Compact* mice show several similarities compared with myostatin knockout animals; however, numerous alterations exist. The *Compact* mutation decreased adiposity and improved insulin sensitivity and glucose uptake, whereas the genetic background exhibited the opposite effect. Importantly, here we show that the mature myostatin protein is present in *Compact* mice, and the 12-bp deletion in the sequence encoding the propeptide decreased the formation of mature myostatin in accordance with increased muscle mass.

MATERIALS AND METHODS

Animals. The *Compact* line carrying the 12-bp deletion in the propeptide of promyostatin (Fig. 1*A*) was selected and inbred in a long-term selection experiment in Berlin, Germany (8, 50). The origin of the Hungarian subpopulation of the *Compact* line was described earlier (3, 22). The BALB/c mice carrying wild-type myostatin were obtained from the Biological Research Centre of the Hungarian Academy of Sciences (Szeged, Hungary). The *Compact* mice were crossed with BALB/c to introgress the wild-type myostatin gene of BALB/c to *Compact* mice. The wild-type myostatin allele was followed through five generations of repeated backcrossing with the *Compact* line. Heterozygous animals of this line in generation B5 were mated inter se to produce homozygous wild-type animals with a *Compact* genetic background (denoted as congenic wild-type animals). Genotyping for *Compact* myostatin mutation [*Mstn(Cmpt-dl1Abc)*] was described earlier (42). Since the *Compact* hypermuscular phenotype is stronger in males than females (47), we performed the study on male 3- to 4-mo-old and 10-mo-old mice. Animal experiments conformed to the National Institutes of Health's *Guide for the Care and Use of Laboratory*

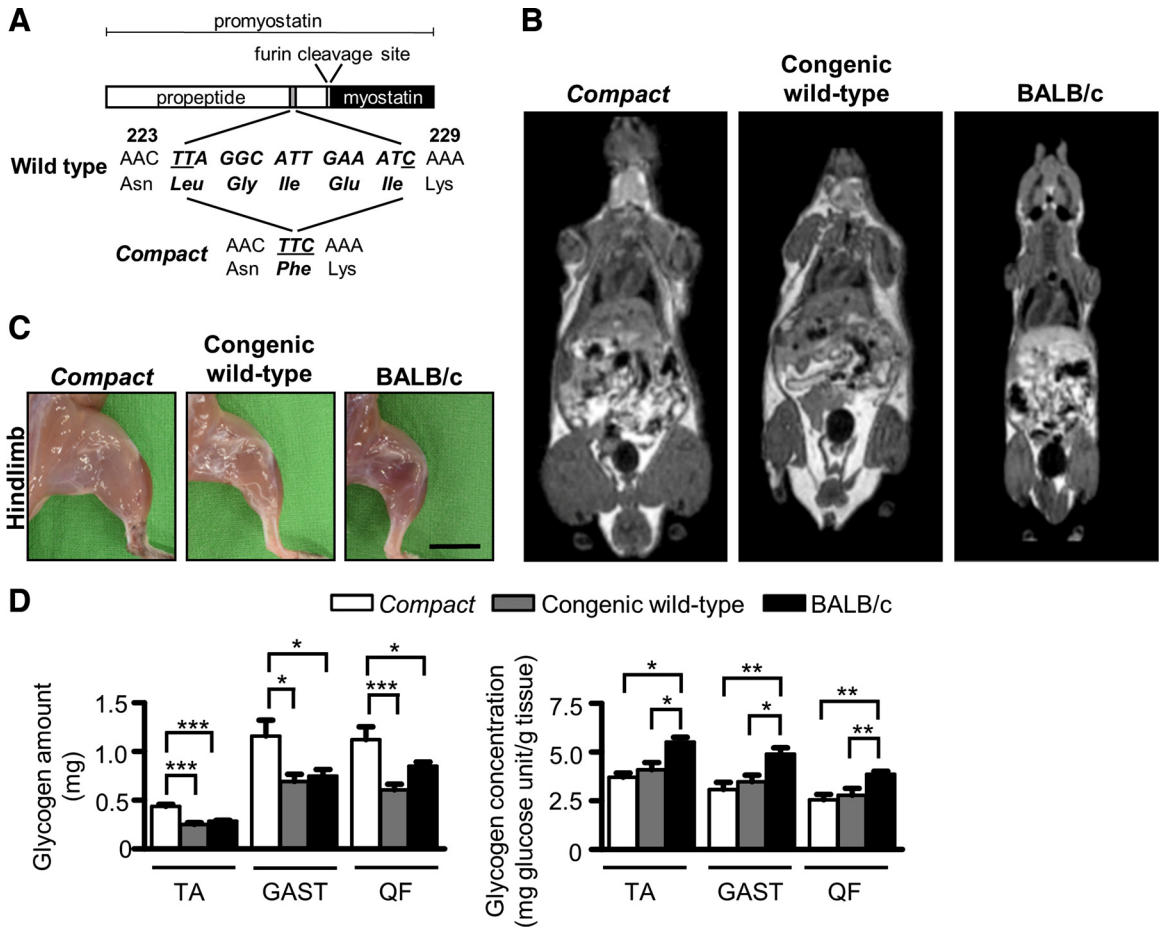

Fig. 1. Characterization of muscle phenotype of *Compact*, congenic wild-type, and BALB/c mice. *A*: schematic representation of the nonframeshift *Compact* mutation in the propeptide region of promyostatin. *B*: representative T1-weighted small-animal MRI images of *Compact*, congenic wild-type, and BALB/c mice. *C*: representative hindlimbs of 4-mo-old mice showing the different muscularity of mice strains. Bar, 10 mm. *D*: total glycogen amount and glycogen concentration (glycogen amount/muscle weight) of hindlimb muscles. Data are presented as means ± SE; $n = 3$ *Compact*, 6 congenic wild-type, and 4 BALB/c mice [m. tibialis anterior (TA)]; $n = 6$ *Compact*, 5 congenic wild-type, and 8 BALB/c mice [m. gastrocnemius (GAST)]; $n = 4$ *Compact*, 6 congenic wild-type, and 9 BALB/c mice [m. quadriceps femoris (QF)]. $^*P < 0.05$; $^{**}P < 0.01$; $^{***}P < 0.001$.

Animals (NIH Publication No. 85-23, revised 1996) and were approved by the local Ethics Committee at the University of Szeged.

Determination of tissue glycogen content. Nonfasting 3- to 4-mo-old male mice were euthanized, and tissues were frozen in liquid nitrogen. Total glycogen amount of the tissue samples was measured as glucose residues by hexokinase/glucose-6-phosphate dehydrogenase assay (Roche) following acidic hydrolysis, as described earlier (22).

Periodic acid Schiff staining. Glycogen content of the liver samples was visualized on 5-μm-thin cryosections by periodic acid Schiff (PAS) staining, as described previously (22).

Measurement of tissue alanine aminotransferase activity. Liver samples of 3- to 4-mo-old male mice were frozen in liquid nitrogen, and tissue homogenates were prepared as described at Western blotting. The activity of alanine aminotransferase (ALT) enzyme of the samples was determined by lactate dehydrogenase-coupled kinetic colorimetric assay (Diagnosticum, Budapest, Hungary) in accordance with the manufacturer's instructions. Spectrophotometry was performed with Fluostar Optima (BMG Labtech, Ortenberg, Germany).

Western blotting. To analyze protein expression levels, m. gastrocnemius and liver samples of 3- to 4-mo-old male animals were homogenized at 4°C in a buffer [50 mM Tris·HCl (pH 7.6), 100 mM NaCl, and 10 mM EDTA] supplemented with protease inhibitor cocktail (Sigma-Aldrich), 1 mM natrium-orthovanadate, and 1 mM natrium-fluoride. Following centrifugation at 4°C for 10 min at 11,000 *g* (Hettich Universal 320R, DJB; Labcare, Buckinghamshire, UK) to remove cellular debris, the protein concentration of the supernatants was determined by BCA kit (Thermo Scientific). The samples were separated on 10% SDS-polyacrylamide gel under reducing or nonreducing conditions and transferred onto Protran nitrocellulose membrane (Amersham, GE Healthcare). After incubation in 5% blocking agent (Bio-Rad), the membrane was incubated with anti-phospho-Akt Ser^{473} (no. 4051; Cell Signaling Technology), anti-phospho-Smad1/5/8 $Ser^{463/465}$ (no. 9511; Cell Signaling Technology), anti-phospho-Smad2 $Ser^{465/467}$ (44-244G; Invitrogen), anti-Smad4 (sc-7966; Santa Cruz Biotechnology), anti-Akt (no. 4691; Cell Signaling Technology), anti-myostatin (AB3239-I; Millipore), anti-GDF8 propeptide (MAB7881; R&D Systems), anti-phospho-AS160 (no. 8881S; Cell Signaling Technology), anti-GLUT4 (no. 2213S; Cell Signaling Technology), or anti-GAPDH (no. 2118; Cell Signaling Technology) primary antibodies, followed by incubation with appropriate horseradish peroxidase-conjugated anti-IgG secondary antibody [P0448 and P0161 (DAKO), 112-035-003 (Jackson Immunoresearch)]. Mouse recombinant myostatin (788-G8; R&D Systems) was used as a positive control. ECL reagent (Advansta, Menlo Park, CA) was used for substrate detection, and the membrane was exposed to X-ray film (AGFA) for visualization.

Intraperitoneal pyruvate tolerance test. Three- to four-month-old male mice were fasted for 16 h before intraperitoneal pyruvate tolerance test and had free access to water. Following the measurement of baseline blood glucose levels, mice were injected with intraperitoneal pyruvate (2 mg pyruvate/1 g body wt). Blood glucose was measured from distal tail vein at 15, 30, 45, 60, 90, and 120 min. All blood glucose measurements were performed by the AccuCheck blood glucose monitoring system (Roche).

Intraperitoneal glucose and insulin tolerance tests. For intraperitoneal glucose tolerance test, male mice were fasted for 16 h and had free access to water. The measurement of baseline blood glucose was followed by intraperitoneal injection of D-glucose (2 mg glucose/1 g body wt), and blood glucose was determined from distal tail vein at 30, 60, 90, and 120 min.

For intraperitoneal insulin tolerance test, animals were fasted for 5 h and had free access to water, and their baseline blood glucose was measured. After the injection of intraperitoneal insulin bolus (1.0 U/1 kg body wt, Humulin R; Eli Lilly, Grootslag, The Netherlands), blood glucose was measured from the distal tail vein at 15, 30, 45, 60, 90, and 120 min. Blood glucose measurements were performed by the AccuCheck blood glucose monitoring system (Roche).

Small-animal PET/MRI imaging using 2-deoxy-2-[^{18}F]fluoro-D-glucose. Ten-month-old male mice were injected with 7.0 ± 0.2 MBq of ^{18}FDG (2-deoxy-2-[^{18}F]fluoro-D-glucose) via the lateral tail vein in 0.2-ml volume. Fifty minutes after ^{18}FDG injection, the animals were anesthetized by 3% isoflurane with a dedicated small-animal anesthesia device, and whole body PET scans (10-min static PET scans) were acquired using the preclinical nanoScan PET/MRI system (Mediso). To prevent movement, animals were fixed to a mouse chamber (MultiCell Imaging Chamber; Mediso) and positioned in the center of the field of view (FOV). For the determination of the anatomic localization of the organs and tissues, T1-weighted MRI scans were performed (3D GRE EXT multi-FOV, TR/TE 15/2 ms, FOV 70 mm, NEX 2). PET volumes were reconstructed using a three-dimensional Ordered Subsets Expectation Maximization (3D-OSEM) algorithm (Tera-Tomo; Mediso). PET and MRI images were automatically coregistered by the PET/MRI instrument's acquisition software (Nucline). Reconstructed, reoriented, and coregistered images were further analyzed with InterView FUSION (Mediso) dedicated image analysis software. Radiotracer uptake was expressed in terms of standardized uptake values (SUVs). Ellipsoidal three-dimensional volumes of interest (VOI) were manually drawn around the edge of the tissue or organ activity by visual inspection using InterView FUSION multimodal visualization and evaluation software (Mediso). The standardized uptake value (SUV) was calculated as follows: SUV = [VOI activity (Bq/ml)]/[injected activity (Bq)/animal weight (g)], assuming a density of 1 g/ml. SUV mean is the average SUV value within the volume of interest (VOI).

Statistical analysis. Statistical evaluations were performed by 1-way ANOVA and Newman-Keuls posttest (GraphPad Software). All data are presented as means ± SE.

RESULTS

Body composition of Compact mice. The body weights of the congenic wild-type mice carrying the wild-type myostatin gene in *Compact* genetic background were higher than those of BALB/c mice, but they were smaller than the *Compact* animals (Table 1). We showed by MRI analysis that profound differences exist in body composition between the genotypes. The qualitative analysis of T1-weighted MRI images revealed remarkable enlargement of skeletal muscle tissues in *Compact* mice. In the MRI images of congenic wild-type animals, the spaciousness of fat tissues was clearly visualized (Fig. 1*B*). The gross enhancement of hindlimb muscle mass was observable (Fig. 1*C*). The absolute weights of individual hindlimb muscles such as tibialis anterior, quadriceps femoris, and gastrocnemius muscles were almost two times greater in *Compact*s compared with congenic wild-type animals, and they were bigger in congenic wild-type animals than in BALB/c mice (Table 1). The muscle weight/body weight ratios showed the highest values in *Compact*s and the lowest in congenic wild-type mice (Table 1).

We found that the absolute weights of heart and kidney of the *Compact* and congenic wild-type mice were comparable and higher than that of BALB/c mice. The absolute weight of abdominal fat increased by ~30% in 3- to 4-mo-old mice and ~50% in 10-mo-old congenic wild-type compared with *Compact*s mice, and it was markedly lower in the BALB/c group than in *Compact*s (Table 2). Liver/body weight ratio of *Compact*s was smaller than that of congenic wild-type animals in both ages (Table 2). Abdominal fat/body weight ratios were comparable in *Compact* and BALB/c animals, and it was

Table 1. *Absolute and normalized muscle weights*

	Compact	Congenic wild-type	BALB/c
		3- to 4-Mo-old animals	
Body weight, g	47.4 ± 0.67[b,e]	40.8 ± 1.76[e]	25.9 ± 0.48
Muscle weight, mg			
TA	113.8 ± 1.64[b,e]	67.6 ± 4.70[e]	45.9 ± 0.88
GAST	350.3 ± 8.15[b,e]	183.9 ± 5.81[e]	140.5 ± 2.14
QF	470.3 ± 12.81[b,e]	246.1 ± 6.71[d]	204.6 ± 3.65
Muscle weight/body weight, mg/g			
TA/body weight	2.4 ± 0.04[b,e]	1.6 ± 0.05[c]	1.8 ± 0.04
GAST/body weight	7.4 ± 0.13[b,e]	4.5 ± 0.11[e]	5.4 ± 0.08
QF/bw	9.9 ± 0.22[b,e]	6.1 ± 0.22[e]	7.9 ± 0.11
		10 Mo old animals	
Body weight, g	50.4 ± 0.53[a,e]	45.1 ± 1.29[e]	31.4 ± 0.88
Muscle weight, mg			
TA	141.8 ± 7.18[b,e]	69.5 ± 2.45[c]	54.3 ± 2.45
GAST	385.4 ± 10.64[b,e]	185.0 ± 2.45[c]	160.5 ± 6.52
QF	476.0 ± 14.09[b,e]	247.5 ± 4.78	221.6 ± 9.43
Muscle weight/body weight, mg/g			
TA/body weight	2.8 ± 0.14[b,e]	1.56 ± 0.08	1.7 ± 0.07
GAST/body weight	7.6 ± 0.1[b,e]	4.13 ± 0.09[e]	5.1 ± 0.11
QF/body weight	9.4 ± 0.22[b,e]	5.52 ± 0.12[e]	7.0 ± 0.12

Values are means ± SE (3- to 4-mo-old animals: $n = 9$ *Compact*, 7 congenic wild-type, and 8 BALB/c mice; 10-mo-old animals: $n = 8$ *Compact*, 12 congenic wild-type, and 8 BALB/c mice). TA, m. tibialis anterior; GAST, m. gastrocnemius; QF, m. quadriceps femoris. The values of the *Compact* group are significantly different from the congenic wild-type group: [a]$P < 0.01$; [b]$P < 0.001$. The values of the *Compact* or congenic wild-type group are significantly different from the BALB/c group: [c]$P < 0.05$; [d]$P < 0.01$; [e]$P < 0.001$.

almost twofold higher in congenic wild-type mice (Table 2). The weights of heart and kidney in proportion to body weight were the smallest in *Compact*s and highest in BALB/c mice (Table 2).

Glycogen accumulation is determined by the genetic background of Compact mice. Myostatin was reported to influence the glycogen content of C2C12 myoblasts (9), and muscle glycogen was reduced in type 2 diabetes mellitus (15). Previously, we have shown that *Compact* tibialis anterior muscle contains more glycogen than that of BALB/c (22). To distinguish the role of *Compact* mutation and the *Compact* genetic background in the regulation of glycogen stores, here we compared the glycogen content of *Compact*, congenic wild-type, and BALB/c muscles. We found that total glycogen levels of *Compact* muscles were the highest, and the congenic wild-type and BALB/c samples contained comparable and smaller amounts of glycogen (Fig. 1*D*). However, the glycogen concentration was the highest in BALB/c mice and displayed no differences between *Compact* and congenic wild-type groups (Fig. 1*D*).

Both the myostatin mutation and *Compact* genetic background influenced liver weight, and liver functions as a glycogen store; therefore, we measured the glycogen content of the liver samples. Analyzing the total glycogen amount and glycogen concentration, we did not observe differences between congenic wild-type and *Compact* groups; the glycogen content/liver weight ratio of BALB/c animals was >2.5-fold smaller (Fig. 2*A*). The visualization of glycogen by PAS staining verified the results of spectrophotometry, and weaker staining was observed in BALB/c samples (Fig. 2*B*).

Liver characteristics in Compact mice. It was reported that knocking out of myostatin results in comparable absolute liver weight, lower liver/body weight ratio, and decreased ALT activity of the liver (18). We found that liver mass and liver/body weight ratios are not increased in proportion to skeletal muscle mass in *Compact* mice; therefore, we aimed to assess whether ALT activity in proportion to body weight is also reduced similarly to myostatin knockout animals. Our data show that total liver ALT activity/body weight ratio was the lowest in *Compact*s and the biggest in BALB/c mice (Table 3).

Table 2. *Absolute and normalized organ weights*

	Compact	Congenic wild-type	BALB/c
		3- to 4-Mo-old animals	
Organ weight, mg			
Liver	1,792.0 ± 43.45[e]	1,874.0 ± 33.68[e]	1,158.0 ± 31.55
Abdominal fat	672.8 ± 59.07[b,d]	1,042.0 ± 105.30[e]	271.9 ± 20.21
Heart	153.8 ± 4.71[d]	163.1 ± 11.41[d]	121.4 ± 3.17
Kidney	237.8 ± 5.97[e]	250.6 ± 11.76[e]	190.4 ± 5.42
Organ weight/body weight, mg/g			
Liver/body weight	37.8 ± 0.81[c,e]	46.3 ± 1.41	44.72 ± 1.04
Abdominal fat/body weight	14.5 ± 1.30[c]	25.3 ± 1.76[e]	10.55 ± 0.89
Heart/body weight	3.3 ± 0.13[c,e]	3.9 ± 0.12[e]	4.68 ± 0.08
Kidney/body weight	5.0 ± 0.11[c,e]	6.16 ± 0.17[e]	7.35 ± 0.17
		10-Mo-old animals	
Organ weight, mg			
Liver	2,037.0 ± 43.15[a,e]	2,213.0 ± 65.05[e]	1,525.0 ± 49.64
Abdominal fat	683.5 ± 35.04[b]	1,236.0 ± 156.3[e]	374.6 ± 41.99
Heart	173.0 ± 3.21[e]	178.2 ± 5.67[e]	140.3 ± 5.11
Kidney	266.9 ± 3.63	300.3 ± 12.03	290.6 ± 21.00
Organ weight/body weight, mg/g			
Liver/body weight	40.4 ± 0.80[c,e]	49.3 ± 1.29	48.6 ± 0.82
Abdominal fat/body weight	13.6 ± 0.75[c]	26.8 ± 2.68[e]	12.1 ± 1.48
Heart/body weight	3.4 ± 0.07[c,e]	3.9 ± 0.07[e]	4.5 ± 0.11
Kidney/body weight	5.3 ± 0.10[a,e]	6.6 ± 0.11[e]	9.3 ± 0.73

Values are means ± SE (3- to 4-mo-old animals: $n = 9$ *Compact*, 7 congenic wild-type, and 8 BALB/c mice; 10-mo-old animals: $n = 8$ *Compact*, 12 congenic wild-type, and 8 BALB/c mice). The values of *Compact* group are significantly different from congenic wild-type group: [a]$P < 0.05$; [b]$P < 0.01$; [c]$P < 0.001$. The values of *Compact* or congenic wild-type group are significantly different from the BALB/c group: [d]$P < 0.01$; [e]$P < 0.001$.

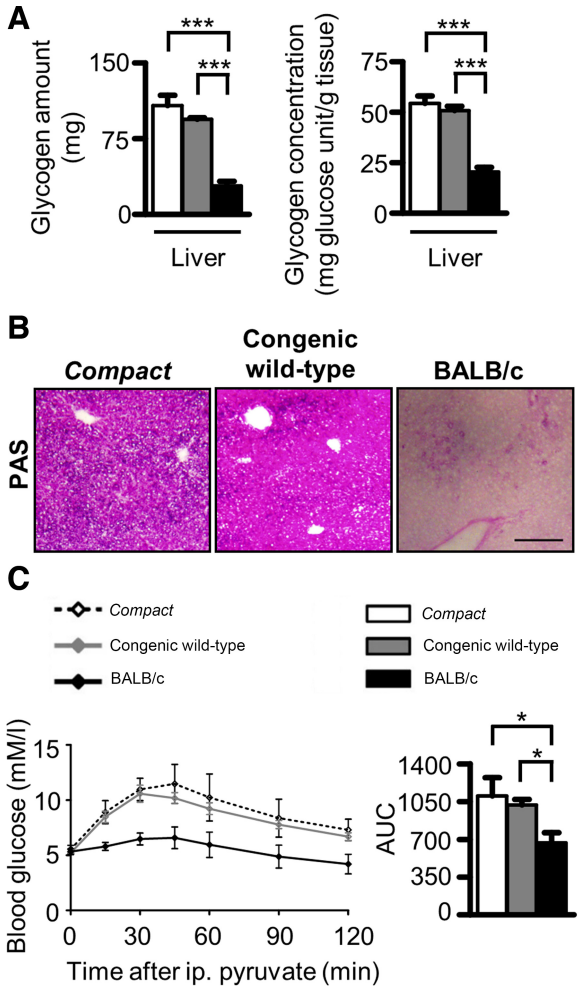

Fig. 2. Characterization of the *Compact*, congenic wild-type, and BALB/c livers. *A*: total glycogen amount and glycogen concentration of the liver samples determined by spectrophotometry ($n = 4$ *Compact*, 5 congenic wild-type, and 4 BALB/c mice). *B*: representative periodic acid Schiff (PAS)-stained images show glycogen content of the liver. Scale bar, 200 μm. *C*: intraperitoneal (ip) pyruvate tolerance test of 3- to 4-mo-old mice ($n = 3$ *Compact*, 5 congenic wild-type, and 4 BALB/c mice). Area under the curve (AUC) values are presented in bar diagrams. Data are reported as means ± SE. $*P < 0.05$; $***P < 0.001$.

Next, we administered glucose precursor pyruvate to measure hepatic gluconeogenesis. The intraperitoneal pyruvate tolerance test showed that hepatic gluconeogenesis increased in *Compact* and congenic wild-type animals compared with BALB/c animals. The area under the curve of blood glucose concentrations during pyruvate tolerance test was comparable in *Compact* and congenic wild-type mice, and it was lower in BALB/c animals (Fig. 2*C*).

The Compact mutation of myostatin propeptide decreases myostatin formation. The *Compact Mstn(Cmpt-dl1Abc)* mutation in the myostatin gene eliminates amino acids 224–228 in the propeptide and creates a new Phe residue (42). The *Compact* mutation is toward the NH_2 terminus from the furin cleavage site, since promyostatin is proteolytically processed by furin at the RSRR (263–266) site to give the active processed myostatin (46). The *Compact* mutation is a nonframeshift 12-bp deletion, and the biologically active growth factor domain is intact; therefore, functional myostatin formation should be permitted. The presence of *Compact* mutation was verified by sequencing the myostatin gene (data not shown). Importantly, we were able to detect mature myostatin dimer in *Compact* skeletal muscle (Fig. 3). Western blot analysis showed that the level of mature myostatin dimer was the lowest in *Compact* muscle and highest in BALB/c mice (Fig. 3) in accordance with the skeletal muscle weights of the animals. The anti-propeptide antibody could recognize the mutant propeptide, and the expression level of propeptide was proportional to myostatin level when the genotypes were compared; the lowest amount was detected in *Compact* samples (Fig. 3).

Effect of Compact myostatin mutation and genetic background on signaling. Myostatin is expressed and secreted predominantly by skeletal muscle; however, as an endocrine factor, it can influence the signal transduction of liver (51). We could detect the mature myostatin; therefore, we investigated myostatin signaling in both skeletal muscle and liver. Despite low levels of myostatin protein in *Compact* skeletal muscle, the level of phospo-Smad2 was the highest when the genotypes were compared (Fig. 4*B*), suggesting the potential role of other TGFβ members in Smad2 activation. The specificity of the anti-p-Smad2 antibody is shown in Fig. 4*A*. Phospho-Smad2 levels of the liver samples were the lowest in BALB/c mice and the highest in *Compact*s (Fig. 4*C*).

Both the Smad2/3 signaling mediated by TGFβ family members and the Smad1/5/8 pathway mediated by bone morphogenic proteins (BMPs) converge on the common mediator Smad4. The balance between these competing pathways is required to maintain muscle mass; the BMP-mediated Smad1/5/8 pathway is the fundamental hypertrophic signal in mice, which is dominant over myostatin signaling, and Smad4 deficiency induces muscle atrophy (37). Furthermore, Smad1/5/8 signaling is an important regulator of liver homeostasis (11, 41). The level of phospho-Smad1/5/8 was significantly higher in muscles of *Compact*s compared with congenic wild-type samples (Fig. 4*B*). However, we have not found any significant differences in phospho-Smad1/5/8 levels of liver samples between the genotypes (Fig. 4*C*). Furthermore, no differences were observed between either muscular (Fig. 4*B*) or hepatic (Fig. 4*C*) Smad4 levels.

Myostatin was reported to inhibit the PI3K/Akt pathway (53); therefore, we determined the phosphorylation level of Akt. The phospho-Akt Ser^{473}/Akt ratio of congenic wild-type liver was lower than that of *Compact* and comparable with

Table 3. *Fasting blood glucose levels and hepatic ALT activity*

	Compact	Congenic wild-type	BALB/c
Fasting blood glucose, mM/l			
3- to 4-Mo-old animals	5.81 ± 0.67	5.81 ± 0.64	5.38 ± 0.69
10-Mo-old animals	5.20 ± 0.25	5.07 ± 0.16	4.82 ± 0.28
Total hepatic ALT activity·g body wt^{-1}, U/g			
3- to 4-mo-old animals	0.12 ± 0.008*‡	0.15 ± 0.006†	0.18 ± 0.002

Values are means ± SE [3- to 4-mo-old animals: $n = 3$ *Compact*, 8 congenic wild-type, and 3 BALB/c mice; 10-mo-old animals: $n = 5$ *Compact*, 3 congenic wild-type, and 6 BALB/c mice for the fasting blood glucose; $n = 4$ in each group for alanine aminotransferase (ALT) activity]. The values of *Compact* group are significantly different from congenic wild-type group: $*P < 0.05$. The values of *Compact* or congenic wild-type group are significantly different from the BALB/c group: $†P < 0.01$; $‡P < 0.001$.

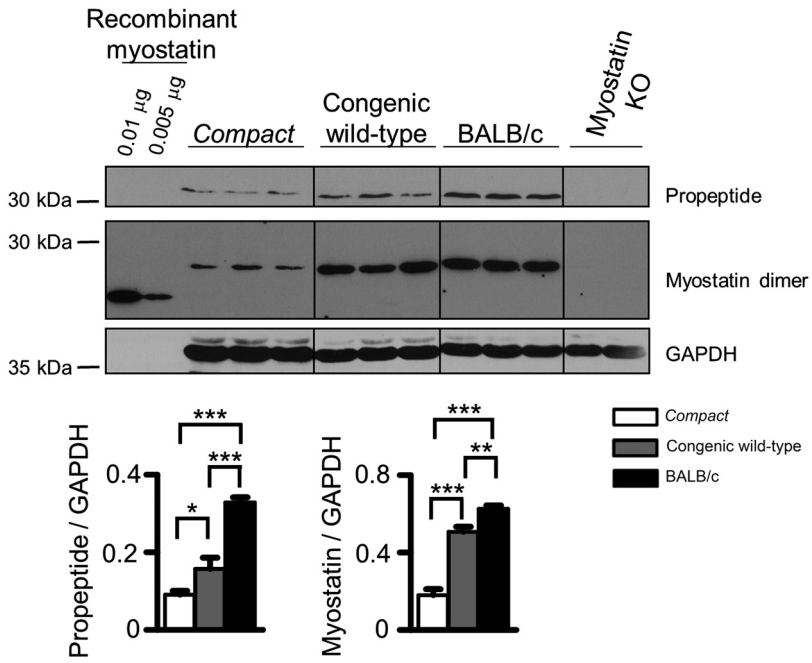

Fig. 3. Myostatin level in skeletal muscle of *Compact*, congenic wild-type, and BALB/c mice. M. gastrocnemius protein extracts were subjected to SDS-PAGE and blotted with anti-myostatin or anti-propeptide antibody. Representative images are shown. Note the presence of mature myostatin dimer and myostatin propeptide in *Compact* samples. Mouse recombinant myostatin was used as a positive control, and muscle homogenates of myostatin knockout (KO) mice served as a negative control. Differences in glycosylation may cause altered electrophoretic mobility. Bar diagrams show the quantification of the results. Data are reported as means ± SE; $n = 5$ *Compact*, 5 congenic wild-type, and 6 BALB/c mice. $^{*}P < 0.05$; $^{**}P < 0.01$; $^{***}P < 0.001$.

BALB/c values (Fig. 4*C*). In contrast, phospho-Akt Ser^{473}/Akt ratios were higher in *Compact* and congenic wild-type muscles compared with BALB/c samples, in accord with myostatin levels (Fig. 4*B*).

AS160 (Akt substrate of 160 kDa), a Rab GTPase-activating protein, can regulate the translocation of GLUT4 glucose transporter to the plasma membrane of insulin-sensitive cells (21). The level of phospho-AS160 was lower in congenic wild-type muscle samples compared with those of *Compact* or BALB/c mice (Fig. 4*D*). The GLUT4 expression showed equal levels in *Compact* and congenic wild-type animals, and the level was lower in BALB/c samples (Fig. 4*D*).

Glucose tolerance and insulin sensitivity are improved by Compact myostatin mutation and reduced by Compact genetic background. As reported previously, knocking out of myostatin increases glucose tolerance and insulin sensitivity (14, 55), and fed and fasting glucose levels in myostatin knockout mice were not significantly different from controls (32). Since the *Compact* mice were hypermuscular and had reduced abdominal fat, we examined whether *Compact* mice showed alterations in glucose metabolism. Because age is reported to influence glucose tolerance (2, 28), we compared whole body glucose tolerance and insulin sensitivity from both young (3- to 4-mo-old) and middle-aged (10-mo-old) groups of mice. Our results did not show any significant changes in fasting blood glucose levels comparing *Compact* mice with age-matched congenic wild-type and BALB/c animals (Table 3); however, the response to exogenous glucose revealed differences between genotypes. *Compact* and BALB/c mice showed greater glucose tolerance compared with age-matched congenic wild-type strain. The area under the curve of blood glucose concentrations during the glucose tolerance test was significantly higher in congenic wild-type mice compared with age-matched *Compact* and BALB/c (Fig. 5*A*). We performed insulin tolerance tests to measure blood glucose changes following insulin administration. Insulin treatment reduced blood glucose levels in all groups of mice, indicating the insulin responsivity. Congenic wild-type mice showed weaker insulin sensitivity compared with *Compact* and BALB/c groups. The area under the curve value during the insulin tolerance test was significantly higher in congenic wild-types than in *Compact* and BALB/c mice at both ages (Fig. 5, *C* and *D*). Both glucose tolerance and insulin sensitivity tests showed comparable results between age-matched *Compacts* and BALB/c mice (Fig. 5, *A–D*).

To test the effect of aging on glucose tolerance and insulin sensitivity, the area under the curve values were compared. The area under the curve of blood glucose concentrations during glucose tolerance tests of 10-mo-old *Compact*s was significantly higher than that of 3- to 4-mo-old animals (1,154 ± 31.5 vs. 943.3 ± 86.3, $P = 0.0318$); no alterations were observed comparing young and middle-aged congenic wild-type or BALB/c groups. The area under the curve values during insulin tolerance tests of young animals were not significantly different from middle-aged groups, although they tended to be smaller in all three genotypes.

Compact mutation increases ^{18}FDG uptake in skeletal muscle, liver, and adipose tissue. The *Compact* mutation and genetic background affected glucose tolerance and insulin sensitivity; therefore, we evaluated glucose uptake in different tissues with known insulin responsiveness using small-animal PET/MRI imaging. By the quantitative analysis of decay-corrected ^{18}FDG-PET images, we found significant differences in the SUV mean of the selected organs 50 min after tracer injection (Fig. 6). The ^{18}FDG accumulation of the skeletal muscle was comparable in *Compact*s and BALB/c animals, and moderate uptake was observed in congenic wild-type animals. The radiotracer uptake of white adipose tissue showed similar results as skeletal muscle, mild uptake was observed in the congenic wild-type mice, and it was approximately twofold higher in *Compact* and BALB/c animals. The liver of *Compact* mice showed the

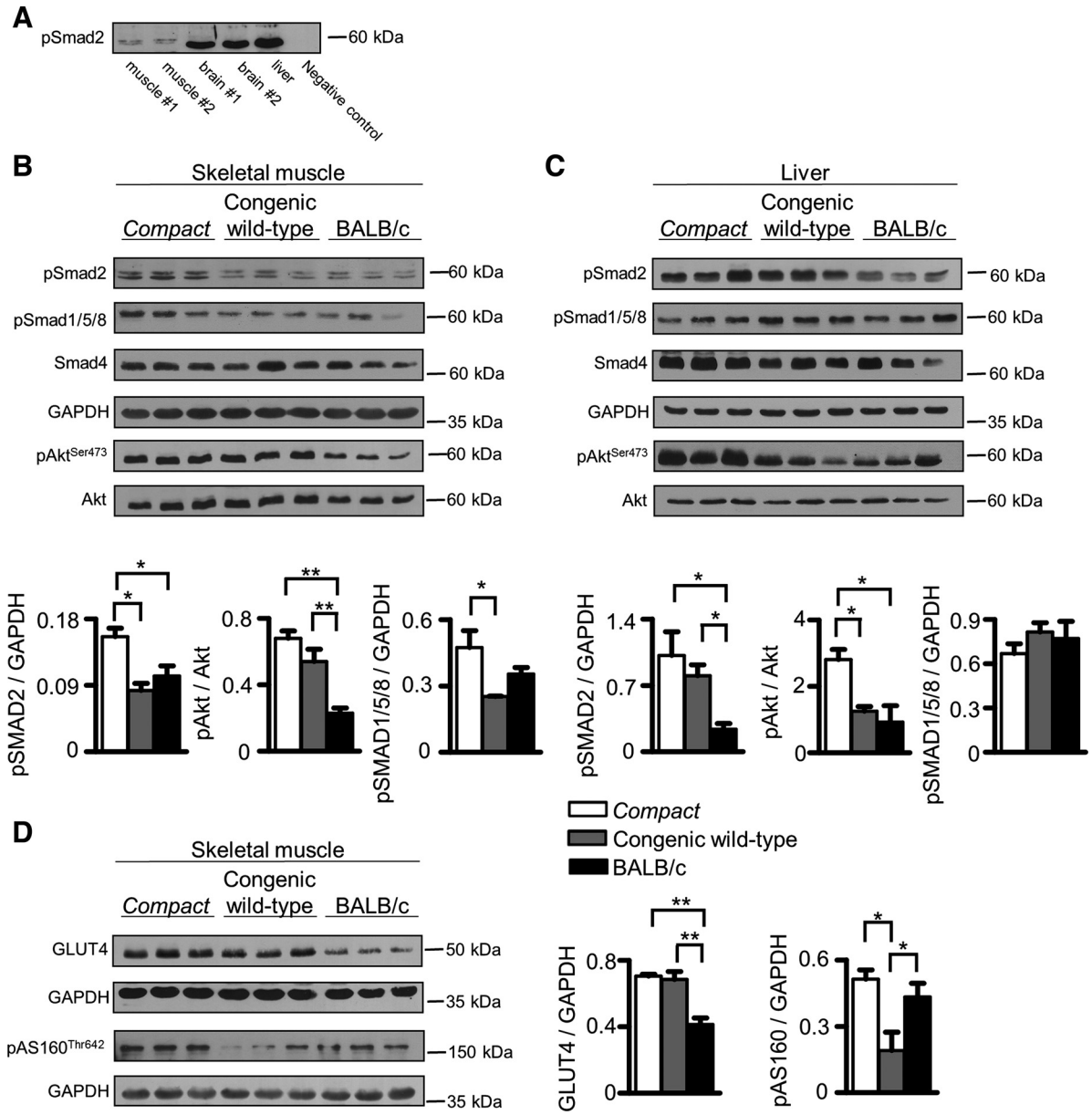

Fig. 4. Alterations of phospho (p)-Smad2, p-Smad1/5/8, p-Akt, and p-AS160 (Akt substrate of 160 kDa) signaling in the different mouse strains. *A*: m. gastrocnemius homogenates (50 μg protein/lane), mouse brain (40 μg protein/lane), and mouse liver (60 μg protein/lane) samples of *Compact* mice were subjected to SDS-PAGE and developed by anti-p-Smad2 antibody to establish the specificity of the antibody. Brain samples served as a positive control, and the negative control was incubated with only the secondary antibody. p-Smad2 was detected at the predicted molecular weight in either mouse skeletal muscle, liver, or positive control samples. Note the low level of p-Smad2 in skeletal muscle compared with liver and brain tissues. *B–D*: Western blot experiments of *Compact*, congenic wild-type, and BALB/c samples indicate the activity of signaling pathways in M. gastrocnemius (*B* and *D*) and liver (*C*) tissues. Bar diagrams show the quantifications of the results. Data are reported as means ± SE; $n = 3$ in each group. *$P < 0.05$; **$P < 0.01$.

highest SUV mean, which was followed by the congenic wild-type and BALB/c groups.

DISCUSSION

Myostatin is a TGFβ family member that is expressed and secreted predominantly by skeletal muscle. The function of myostatin appears to be conserved across species, since mutations in the myostatin gene induce bigger muscles in human, mice, cattle, dogs, and sheep (10, 20, 37, 38, 42). The *Compact* mice arose during a long-term selection program to reach the maximal hypermuscularity (7). The major gene responsible for the hypermuscular phenotype was mapped on chromosome 1 (49), and after the discovery of myostatin gene (31) the *Mstn(Cmpt-dl1Abc)* deletion in the propeptide region of the mouse myostatin was identified as the causative mutation responsible for the *Compact* phenotype (47). Due to selection for hypermuscularity, the *Compact* line, in addition to achieving homozygosity for the *Mstn(Cmpt-dl1Abc)* mutation, also accumulated modifier alleles that were involved in the full expression of the phenotype (47, 48). Markers on several chromosomes (chromosomes 1, 3, 5, 7, 11, 16, and X) showed linkage with the putative modifiers, and the strongest associa-

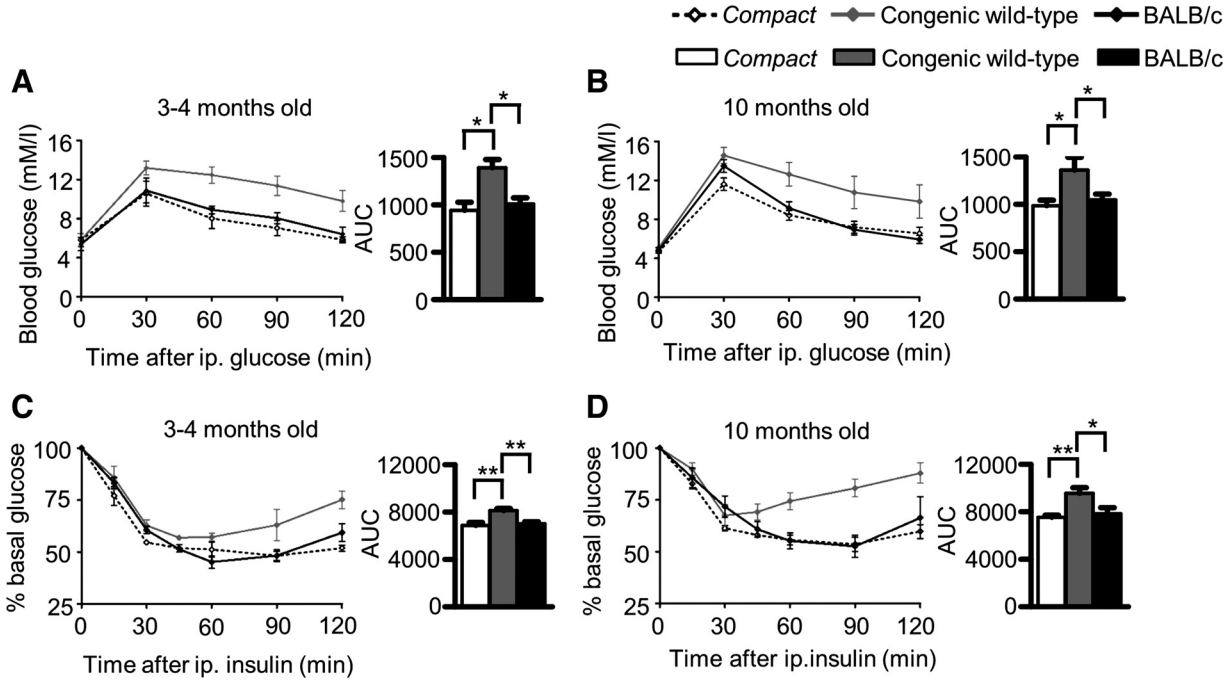

Fig. 5. Glucose tolerance and insulin sensitivity are improved by *Compact* myostatin mutation and reduced in congenic wild-type mice. Intraperitoneal (ip) glucose tolerance (*A* and *B*) and insulin sensitivity tests (*C* and *D*) of 3- to 4-mo-old (*A* and *C*) and 10-mo-old animals (*B* and *D*). Area under the curve (AUC) values are presented in bar diagrams. Data are reported as means ± SE. $^{*}P < 0.05$ and $^{**}P < 0.01$; $n = 3$ *Compact*, 7 congenic wild-type, and 3 BALB/c mice (*A*), $n = 7$ *Compact*, 3 congenic wild-type, and 6 BALB/c mice (*B*), $n = 3$ *Compact*, 3 congenic wild-type, and 4 BALB/c mice (*C*), and $n = 6$ *Compact*, 4 congenic wild-type, and 4 BALB/c mice (*D*).

tion was found for markers on chromosomes 16 and X (47, 48). Myogenin is a candidate on chromosome 1 (48), which has been proposed as a downstream target of myostatin (23). Candidates localized on chromosome 7 are MyoD1, a key regulator of myogenesis, and Pcsk6 (protein convertase subtilisin/kexin type 6), which is involved in proteolytic processing of TGFβ members. Further candidates are chordin on chromosome 16, which binds BMPs and sequesters them in a latent complex, and androgen receptor on chromosome X (47).

Moreover, little is known about the detailed phenotype of *Compact* mice, and the molecular consequences of *Compact* mutation are completely unclear. We and others have reported earlier that the *Compact* mice are hypermuscular (3, 22, 35), and cellularity of the *Compact* skeletal muscles shows increased ratio of glycolytic fibers in rectus femoris, longissimus dorsi (35), and tibialis anterior (3, 22) muscles. Decreased specific force (1) and reduced calcium release from sarcoplasmic reticulum (5) were reported in *Compact* muscles.

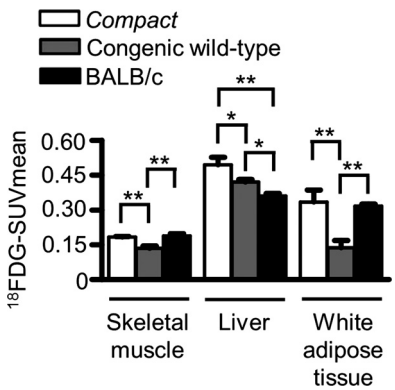

Fig. 6. *Compact* mutation increases ^{18}FDG (2-deoxy-2-[^{18}F]fluoro-D-glucose) uptake. Quantitative analysis of ^{18}FDG uptake of selected tissues in *Compact*, congenic, and BALB/c mice 50 min after tracer injection. Data are presented as means ± SE; $n = 3$ *Compact*, 4 congenic wild-type, and 4 BALB/c mice (skeletal muscle, liver); $n = 4$ in each group (white adipose tissue). $^{*}P < 0.05$; $^{**}P < 0.01$.

To separately study the effect of *Compact* myostatin mutation and *Compact* genetic background, we generated a congenic wild-type strain carrying wild-type myostatin in the *Compact* genetic background. We introgressed the wild-type myostatin gene of BALB/c to *Compact* mice to generate the congenic wild-type line, and we used BALB/c mice as a wild-type control for the reasons listed by Baán et al. (3). Briefly, this inbred line was used for mapping the *Compact* myostatin mutation and the modifier genes (42), and their muscle characteristics are similar to those of C57BL/6 mice. We have found that both the *Compact* myostatin mutation and the *Compact* genetic background account for determination of skeletal muscle size. The *Compact* mutation resulted in a disproportionate increase in skeletal muscle mass, leading to increased muscle/body weight ratios and decreased internal organ/body weight ratios. The *Compact* mice are weighted and hypermuscular compared with both congenic wild-type and BALB/c animals. Interestingly, the normalized muscle weights of congenic wild-type animals are the smallest despite their increased absolute muscle weights compared with BALB/c mice; therefore, other organs should be involved in accretion of body weight of congenic wild-type animals.

Beyond the regulation of muscularity, myostatin was shown earlier to influence the size of internal organs. Knocking out of myostatin resulted in decreased weight of fat, liver, and kidney

as proportional to body weight (18, 19, 26, 32). The absolute weight of heart increased; however, heart weight/body weight ratio did not change (19, 26). Bünger et al. (8) introgressed the *Compact* mutation into a mouse line with extreme growth (DUHi). The *Compact* mutation in the DUHi background decreased the absolute size of liver, heart, and kidney (8); in contrast, based on our study, the *Compact* mutation did not affect them in the *Compact* background, indicating the importance of genetic background in the manifestation of the phenotype. However, the *Compact* mutation resulted in hypermuscularity in both the DUHi (8) and *Compact* backgrounds as well. Similarly to myostatin knockouts, the liver/body weight ratio set point is reduced in *Compact*s. By testing the enzymatic functions of the liver, despite the smaller liver weight/body weight ratio of *Compact*s, the hepatic gluconeogenesis was comparable with congenic wild-type animals following exogenous pyruvate. The tissue ALT activity of the liver was reduced by *Compact* myostatin mutation similarly to knocking out of myostatin (18).

Myostatin was reported to affect glucose metabolism; however, the fed and fasting glucose levels of myostatin knockout male mice were not different from controls (32). Similarly to these observations, fasting blood glucose levels of *Compact* mice did not change compared with age-matched congenic wild-type and BALB/c animals. Furthermore, myostatin-null mice have reduced body fat beyond the increased muscle mass and exhibit increased insulin sensitivity (14, 55). Here, we showed that *Compact* mutation increased muscularity and decreased adiposity similarly to myostatin knockout mice, whereas the genetic background had the opposite effect, increasing adiposity and decreasing skeletal muscle mass/body weight ratios. As a consequence of these alterations in body composition, the *Compact* mutation improved whole body glucose tolerance and insulin sensitivity, whereas the genetic background decreased them. The *Compact* mutation increased the ^{18}FDG radiotracer uptake into all investigated organs (white adipose tissue, skeletal muscle, and liver). The phosphorylation of AS160 was shown to regulate the translocation of GLUT4 to the plasma membrane (21, 36). However, the *Compact* mutation did not influence the amount of GLUT4 in skeletal muscle, but the increased p-AS160 level in *Compact* animals might contribute to the increased glucose uptake by enhancing the GLUT4 translocation to the plasma membrane.

Besides the regulation of insulin sensitivity and glucose tolerance, the *Compact* genetic background has a role in the regulation of tissue glycogen content. It has opposite impacts on skeletal muscle and liver by decreasing the glycogen level/tissue weight ratio in muscle and increasing it in the liver. These alterations can be at least partially the consequences of decreased glucose uptake into muscle and increased glucose uptake into liver. Consistent with these results, reduced muscle glycogen was reported in type 2 diabetes mellitus (15). The *Compact* mutation itself did not affect the glycogen level/tissue weight ratio in either muscle or liver tissue; however, myostatin treatment was found to reduce the glycogen content of C2C12 myoblasts (9).

Age was shown to affect glucose metabolism; however, no difference was reported in glucose clearance rate comparing 6- and 12-mo-old BALB/c mice (33). Consistent with these results, the glucose tolerance of BALB/c animals did not change with age (3–4 vs. 10 mo old) in our study. Interestingly, aging reduced glucose tolerance of *Compact* mice without any significant alteration in sensitivity for exogenous insulin.

Although the *Compact* mutation was identified in 1998 (42), its precise molecular effects have not yet been published. The *Compact* mutation is a nonframeshift deletion in the propeptide; therefore, it raised the possibility that the mature myostatin is present in *Compact* mice. Here, we have shown that the *Compact* mutation allows the formation of mature myostatin; however, the amount of myostatin was lower in *Compact* skeletal muscle, in accordance with increased muscle mass. Most of the naturally occurring myostatin mutations led to the development of an early STOP codon; however, some mutations were shown to be associated with altered proteolysis of promyostatin (4, 43) permitting myostatin formation.

The specific functions of the propeptides of TGF superfamily members are largely unknown; however, they can play a role in targeting and inactivation of the biological active COOH-terminal part, and they have an impact on binding properties to extracellular components. All of these functions of myostatin propeptide can be disturbed by *Compact* mutation. It was reported that BMP-7 propeptide binds fibrillin-1 (39), BMP-5 propeptide binds fibrillin-1 and -2 (39), and the interaction between myostatin propeptide and perlecan was identified (40). The interaction of propeptide and myostatin is relevant in vivo, with a majority (>70%) of myostatin in serum bound to its propeptide (16). The amino acid sequence of GDF-11 (growth/differentiation factor-11) is 90% homologous to myostatin in the carboxy-terminal mature region of the protein, and like myostatin, GDF-11 can signal through ActRIIB (30), and GDF-11 administration leads to activation of Smad2 signaling (12, 34). Myostatin propeptide may bind and inhibit GDF-11 as well as myostatin (30); therefore, the mutant propeptide of *Compact* mice might disturb not only myostatin but, e.g., GDF-11 signaling as well.

Despite the low level of myostatin protein in *Compact* skeletal muscle, the level of phospo-Smad2 was the highest when the genotypes were compared, suggesting the potential role of other TGFβ members (e.g., GDF-11) or HGF (hepatocyte growth factor) in Smad2 activation. HGF is a regulator of satellite cells (44) and transmits signals through Smad2/3. The BMP-mediated Smad1/5/8 signaling is an important regulator of skeletal muscle mass (37, 52), hepatocyte proliferation, and liver regeneration and function (11, 41). Comparing the genotypes, phospho-Smad1/5/8 levels show the same pattern as tissue weight/body weight ratios in both skeletal muscle and liver, suggesting the impact of Smad1/5/8 signaling on regulation of skeletal muscle and liver size. The BMP inhibitor chordin was proposed as a modifier gene in *Compact* mice (48) that can influence the activity of BMP pathway by binding and modulating the effect of BMPs (54). Interestingly, the elevated phospho-Smad1/5/8 levels can derive not just from BMPs, since TGFβ was reported to stimulate the phosphorylation of Smad1/5 through a noncanonical mechanism (27).

The *Compact* mice represent a complex system consisting of a natural mutation in the propeptide of promyostatin and additional modifier genes. The *Compact* mice show several similarities compared with myostatin knockout animals; however, numerous alterations exist due to the redundant function of propeptide and the presence of the specific *Compact* genetic background. Myostatin propeptide may bind and inhibit GDF-11 as well (30); therefore, the effect of *Compact* propep-

tide cannot be restricted to myostatin signaling. Our analysis has shown that the modifier genes of the genetic background can strengthen the effect of *Compact* myostatin mutation, or they can compensate for each other. Further analysis of the biological effect of *Compact* mutation and the identification of modifier genes may provide a route to additional upstream and downstream factors involved in the regulation of skeletal muscle size and metabolism.

ACKNOWLEDGMENTS

We thank Zita Makrane Felho and Laszlone Csontos for excellent technical assistance. We thank Jozsef Mihaly for providing horseradish peroxidase-conjugated anti-rat secondary antibody.

GRANTS

This research was supported by the European Union and the State of Hungary and cofinanced by the European Social Fund in the framework of the TÁMOP 4.2.4. A/2-11-1-2012-0001 "National Excellence Program" (to A. Keller-Pinter) and GINOP-2.3.2-15-2016-00006.

DISCLOSURES

No conflicts of interest, financial or otherwise, are declared by the authors.

AUTHOR CONTRIBUTIONS

T.K., G.T., K.S., and A.K.-P. performed experiments; T.K., G.T., and A.K.-P. analyzed data; T.K., G.T., J.A.B., and A.K.-P. interpreted results of experiments; T.K. and A.K.-P. prepared figures; T.K., G.T., L.M., I.G., H.R., F.D., and A.K.-P. drafted manuscript; T.K., F.D., L.D., and A.K.-P. edited and revised manuscript; T.K., G.T., K.S., J.A.B., G.M., L.M., I.G., H.R., F.D., L.D., and A.K.-P. approved final version of manuscript.

REFERENCES

1. **Amthor H, Macharia R, Navarrete R, Schuelke M, Brown SC, Otto A, Voit T, Muntoni F, Vrbóva G, Partridge T, Zammit P, Bunger L, Patel K.** Lack of myostatin results in excessive muscle growth but impaired force generation. *Proc Natl Acad Sci USA* 104: 1835–1840, 2007. doi:10.1073/pnas.0604893104.
2. **Ayala JE, Samuel VT, Morton GJ, Obici S, Croniger CM, Shulman GI, Wasserman DH, McGuinness OP; NIH Mouse Metabolic Phenotyping Center Consortium.** Standard operating procedures for describing and performing metabolic tests of glucose homeostasis in mice. *Dis Model Mech* 3: 525–534, 2010. doi:10.1242/dmm.006239.
3. **Baán JA, Kocsis T, Keller-Pintér A, Müller G, Zádor E, Dux L, Mendler L.** The compact mutation of myostatin causes a glycolytic shift in the phenotype of fast skeletal muscles. *J Histochem Cytochem* 61: 889–900, 2013. doi:10.1369/0022155413503661.
4. **Berry C, Thomas M, Langley B, Sharma M, Kambadur R.** Single cysteine to tyrosine transition inactivates the growth inhibitory function of Piedmontese myostatin. *Am J Physiol Cell Physiol* 283: C135–C141, 2002. doi:10.1152/ajpcell.00458.2001.
5. **Bodnár D, Geyer N, Ruzsnavszky O, Oláh T, Hegyi B, Sztretye M, Fodor J, Dienes B, Balogh Á, Papp Z, Szabó L, Müller G, Csernoch L, Szentesi P.** Hypermuscular mice with mutation in the myostatin gene display altered calcium signalling. *J Physiol* 592: 1353–1365, 2014. doi:10.1113/jphysiol.2013.261958.
6. **Brandt C, Hansen RH, Hansen JB, Olsen CH, Galle P, Mandrup-Poulsen T, Gehl J, Pedersen BK, Hojman P.** Over-expression of Follistatin-like 3 attenuates fat accumulation and improves insulin sensitivity in mice. *Metabolism* 64: 283–295, 2015. doi:10.1016/j.metabol.2014.10.007.
7. **Bünger L, Laidlaw A, Bulfield G, Eisen EJ, Medrano JF, Bradford GE, Pirchner F, Renne U, Schlote W, Hill WG.** Inbred lines of mice derived from long-term growth selected lines: unique resources for mapping growth genes. *Mamm Genome* 12: 678–686, 2001. doi:10.1007/s00335001-3018-6.
8. **Bünger L, Ott G, Varga L, Schlote W, Rehfeldt C, Renne U, Williams JL, Hill WG.** Marker-assisted introgression of the Compact mutant myostatin allele MstnCmpt-dl1Abc into a mouse line with extreme growth effects on body composition and muscularity. *Genet Res* 84: 161–173, 2004. doi:10.1017/S0016672304007165.
9. **Chen Y, Ye J, Cao L, Zhang Y, Xia W, Zhu D.** Myostatin regulates glucose metabolism via the AMP-activated protein kinase pathway in skeletal muscle cells. *Int J Biochem Cell Biol* 42: 2072–2081, 2010. doi:10.1016/j.biocel.2010.09.017.
10. **Clop A, Marcq F, Takeda H, Pirottin D, Tordoir X, Bibé B, Bouix J, Caiment F, Elsen JM, Eychenne F, Larzul C, Laville E, Meish F, Milenkovic D, Tobin J, Charlier C, Georges M.** A mutation creating a potential illegitimate microRNA target site in the myostatin gene affects muscularity in sheep. *Nat Genet* 38: 813–818, 2006. doi:10.1038/ng1810.
11. **Do N, Zhao R, Ray K, Ho K, Dib M, Ren X, Kuzontkoski P, Terwilliger E, Karp SJ.** BMP4 is a novel paracrine inhibitor of liver regeneration. *Am J Physiol Gastrointest Liver Physiol* 303: G1220–G1227, 2012. doi:10.1152/ajpgi.00105.2012.
12. **Egerman MA, Cadena SM, Gilbert JA, Meyer A, Nelson HN, Swalley SE, Mallozzi C, Jacobi C, Jennings LL, Clay I, Laurent G, Ma S, Brachat S, Lach-Trifilieff E, Shavlakadze T, Trendelenburg AU, Brack AS, Glass DJ.** GDF11 Increases with Age and Inhibits Skeletal Muscle Regeneration. *Cell Metab* 22: 164–174, 2015. doi:10.1016/j.cmet.2015.05.010.
13. **Guo T, Bond ND, Jou W, Gavrilova O, Portas J, McPherron AC.** Myostatin inhibition prevents diabetes and hyperphagia in a mouse model of lipodystrophy. *Diabetes* 61: 2414–2423, 2012. doi:10.2337/db11-0915.
14. **Guo T, Jou W, Chanturiya T, Portas J, Gavrilova O, McPherron AC.** Myostatin inhibition in muscle, but not adipose tissue, decreases fat mass and improves insulin sensitivity. *PLoS One* 4: e4937, 2009. doi:10.1371/journal.pone.0004937.
15. **He J, Kelley DE.** Muscle glycogen content in type 2 diabetes mellitus. *Am J Physiol Endocrinol Metab* 287: E1002–E1007, 2004. doi:10.1152/ajpendo.00015.2004.
16. **Hill JJ, Davies MV, Pearson AA, Wang JH, Hewick RM, Wolfman NM, Qiu Y.** The myostatin propeptide and the follistatin-related gene are inhibitory binding proteins of myostatin in normal serum. *J Biol Chem* 277: 40735–40741, 2002. doi:10.1074/jbc.M206379200.
17. **Hittel DS, Berggren JR, Shearer J, Boyle K, Houmard JA.** Increased secretion and expression of myostatin in skeletal muscle from extremely obese women. *Diabetes* 58: 30–38, 2009. doi:10.2337/db08-0943.
18. **Huang J, Glauber M, Qiu Z, Gazit V, Dietzen DJ, Rudnick DA.** The influence of skeletal muscle on the regulation of liver:body mass and liver regeneration. *Am J Pathol* 180: 575–582, 2012. doi:10.1016/j.ajpath.2011.10.032.
19. **Jackson MF, Luong D, Vang DD, Garikipati DK, Stanton JB, Nelson OL, Rodgers BD.** The aging myostatin null phenotype: reduced adiposity, cardiac hypertrophy, enhanced cardiac stress response, and sexual dimorphism. *J Endocrinol* 213: 263–275, 2012. doi:10.1530/JOE-11-0455.
20. **Kambadur R, Sharma M, Smith TP, Bass JJ.** Mutations in myostatin (GDF8) in double-muscled Belgian Blue and Piedmontese cattle. *Genome Res* 7: 910–916, 1997.
21. **Klip A, Sun Y, Chiu TT, Foley KP.** Signal transduction meets vesicle traffic: the software and hardware of GLUT4 translocation. *Am J Physiol Cell Physiol* 306: C879–C886, 2014. doi:10.1152/ajpcell.00069.2014.
22. **Kocsis T, Baán J, Müller G, Mendler L, Dux L, Keller-Pintér A.** Skeletal muscle cellularity and glycogen distribution in the hypermuscular Compact mice. *Eur J Histochem* 58: 2353, 2014. doi:10.4081/ejh.2014.2353.
23. **Langley B, Thomas M, Bishop A, Sharma M, Gilmour S, Kambadur R.** Myostatin inhibits myoblast differentiation by down-regulating MyoD expression. *J Biol Chem* 277: 49831–49840, 2002. doi:10.1074/jbc.M204291200.
24. **Lee SJ, McPherron AC.** Regulation of myostatin activity and muscle growth. *Proc Natl Acad Sci USA* 98: 9306–9311, 2001. doi:10.1073/pnas.151270098.
25. **Li Z, Zhao B, Kim YS, Hu CY, Yang J.** Administration of a mutated myostatin propeptide to neonatal mice significantly enhances skeletal muscle growth. *Mol Reprod Dev* 77: 76–82, 2010. doi:10.1002/mrd.21111.
26. **Lin J, Arnold HB, Della-Fera MA, Azain MJ, Hartzell DL, Baile CA.** Myostatin knockout in mice increases myogenesis and decreases adipogenesis. *Biochem Biophys Res Commun* 291: 701–706, 2002. doi:10.1006/bbrc.2002.6500.
27. **Liu IM, Schilling SH, Knouse KA, Choy L, Derynck R, Wang XF.** TGFbeta-stimulated Smad1/5 phosphorylation requires the ALK5 L45 loop and mediates the pro-migratory TGFbeta switch. *EMBO J* 28: 88–98, 2009. doi:10.1038/emboj.2008.266.

28. **Mathew D, Zhou P, Pywell CM, van der Veen DR, Shao J, Xi Y, Bonar NA, Hummel AD, Chapman S, Leevy WM, Duffield GE.** Ablation of the ID2 gene results in altered circadian feeding behavior, and sex-specific enhancement of insulin sensitivity and elevated glucose uptake in skeletal muscle and brown adipose tissue. *PLoS One* 8: e73064, 2013. doi:10.1371/journal.pone.0073064.
29. **McCroskery S, Thomas M, Maxwell L, Sharma M, Kambadur R.** Myostatin negatively regulates satellite cell activation and self-renewal. *J Cell Biol* 162: 1135–1147, 2003. doi:10.1083/jcb.200207056.
30. **McPherron AC.** Metabolic functions of myostatin and GDF11. *Immunol Endocr Metab Agents Med Chem* 10: 217–231, 2010. doi:10.2174/187152210793663810.
31. **McPherron AC, Lawler AM, Lee SJ.** Regulation of skeletal muscle mass in mice by a new TGF-beta superfamily member. *Nature* 387: 83–90, 1997. doi:10.1038/387083a0.
32. **McPherron AC, Lee SJ.** Suppression of body fat accumulation in myostatin-deficient mice. *J Clin Invest* 109: 595–601, 2002. doi:10.1172/JCI0213562.
33. **Nankervis SA, Mitchell JM, Charchar FJ, McGlynn MA, Lewandowski PA.** Consumption of a low glycaemic index diet in late life extends lifespan of Balb/c mice with differential effects on DNA damage. *Longev Healthspan* 2: 4, 2013. doi:10.1186/2046-2395-2-4.
34. **Poggioli T, Vujic A, Yang P, Macias-Trevino C, Uygur A, Loffredo FS, Pancoast JR, Cho M, Goldstein J, Tandias RM, Gonzalez E, Walker RG, Thompson TB, Wagers AJ, Fong YW, Lee RT.** Circulating growth differentiation factor 11/8 levels decline with Age. *Circ Res* 118: 29–37, 2016. doi:10.1161/CIRCRESAHA.115.307521.
35. **Rehfeldt C, Ott G, Gerrard DE, Varga L, Schlote W, Williams JL, Renne U, Bünger L.** Effects of the compact mutant myostatin allele Mstn (Cmpt-dl1Abc) introgressed into a high growth mouse line on skeletal muscle cellularity. *J Muscle Res Cell Motil* 26: 103–112, 2005. doi:10.1007/s10974-005-1099-7.
36. **Sakamoto K, Holman GD.** Emerging role for AS160/TBC1D4 and TBC1D1 in the regulation of GLUT4 traffic. *Am J Physiol Endocrinol Metab* 295: E29–E37, 2008. doi:10.1152/ajpendo.90331.2008.
37. **Sartori R, Schirwis E, Blaauw B, Bortolanza S, Zhao J, Enzo E, Stantzou A, Mouisel E, Toniolo L, Ferry A, Stricker S, Goldberg AL, Dupont S, Piccolo S, Amthor H, Sandri M.** BMP signaling controls muscle mass. *Nat Genet* 45: 1309–1318, 2013. doi:10.1038/ng.2772.
38. **Schuelke M, Wagner KR, Stolz LE, Hübner C, Riebel T, Kömen W, Braun T, Tobin JF, Lee SJ.** Myostatin mutation associated with gross muscle hypertrophy in a child. *N Engl J Med* 350: 2682–2688, 2004. doi:10.1056/NEJMoa040933.
39. **Sengle G, Charbonneau NL, Ono RN, Sasaki T, Alvarez J, Keene DR, Bächinger HP, Sakai LY.** Targeting of bone morphogenetic protein growth factor complexes to fibrillin. *J Biol Chem* 283: 13874–13888, 2008. doi:10.1074/jbc.M707820200.
40. **Sengle G, Ono RN, Sasaki T, Sakai LY.** Prodomains of transforming growth factor β (TGFβ) superfamily members specify different functions: extracellular matrix interactions and growth factor bioavailability. *J Biol Chem* 286: 5087–5099, 2011. doi:10.1074/jbc.M110.188615.
41. **Sugimoto H, Yang C, LeBleu VS, Soubasakos MA, Giraldo M, Zeisberg M, Kalluri R.** BMP-7 functions as a novel hormone to facilitate liver regeneration. *FASEB J* 21: 256–264, 2006. doi:10.1096/fj.06-6837com.
42. **Szabó G, Dallmann G, Müller G, Patthy L, Soller M, Varga L.** A deletion in the myostatin gene causes the compact (Cmpt) hypermuscular mutation in mice. *Mamm Genome* 9: 671–672, 1998. doi:10.1007/s003359900843.
43. **Szláma G, Trexler M, Buday L, Patthy L.** K153R polymorphism in myostatin gene increases the rate of promyostatin activation by furin. *FEBS Lett* 589: 295–301, 2015. doi:10.1016/j.febslet.2014.12.011.
44. **Tatsumi R, Anderson JE, Nevoret CJ, Halevy O, Allen RE.** HGF/SF is present in normal adult skeletal muscle and is capable of activating satellite cells. *Dev Biol* 194: 114–128, 1998. doi:10.1006/dbio.1997.8803.
45. **Thies RS, Chen T, Davies MV, Tomkinson KN, Pearson AA, Shakey QA, Wolfman NM.** GDF-8 propeptide binds to GDF-8 and antagonizes biological activity by inhibiting GDF-8 receptor binding. *Growth Factors* 18: 251–259, 2001. doi:10.3109/08977190109029114.
46. **Thomas M, Langley B, Berry C, Sharma M, Kirk S, Bass J, Kambadur R.** Myostatin, a negative regulator of muscle growth, functions by inhibiting myoblast proliferation. *J Biol Chem* 275: 40235–40243, 2000. doi:10.1074/jbc.M004356200.
47. **Varga L, Müller G, Szabó G, Pinke O, Korom E, Kovács B, Patthy L, Soller M.** Mapping modifiers affecting muscularity of the myostatin mutant (Mstn(Cmpt-dl1Abc)) compact mouse. *Genetics* 165: 257–267, 2003.
48. **Varga L, Pinke O, Müller G, Kovács B, Korom E, Szabó G, Soller M.** Mapping a syntenic modifier on mouse chromosome 1 influencing the expressivity of the compact phenotype in the myostatin mutant (MstnCmpt-dl1Abc) compact mouse. *Genetics* 169: 489–493, 2005. doi:10.1534/genetics.104.034033.
49. **Varga L, Szabó G, Darvasi A, Müller G, Sass M, Soller M.** Inheritance and mapping of Compact (Cmpt), a new mutation causing hypermuscularity in mice. *Genetics* 147: 755–764, 1997.
50. **Weniger JH, Horst P, Steinhauf D, Major F, Wolf M, Tawfik ES.** Model experiments on selection for endurance and its relation to growth. Part I. Introduction, methods and preliminary investigations on the basic population. *J Anim Breed Genet* 91: 265–270, 1974.
51. **Williams NG, Interlichia JP, Jackson MF, Hwang D, Cohen P, Rodgers BD.** Endocrine actions of myostatin: systemic regulation of the IGF and IGF binding protein axis. *Endocrinology* 152: 172–180, 2011. doi:10.1210/en.2010-0488.
52. **Winbanks CE, Chen JL, Qian H, Liu Y, Bernardo BC, Beyer C, Watt KI, Thomson RE, Connor T, Turner BJ, McMullen JR, Larsson L, McGee SL, Harrison CA, Gregorevic P.** The bone morphogenetic protein axis is a positive regulator of skeletal muscle mass. *J Cell Biol* 203: 345–357, 2013. doi:10.1083/jcb.201211134.
53. **Yang W, Zhang Y, Li Y, Wu Z, Zhu D.** Myostatin induces cyclin D1 degradation to cause cell cycle arrest through a phosphatidylinositol 3-kinase/AKT/GSK-3 beta pathway and is antagonized by insulin-like growth factor 1. *J Biol Chem* 282: 3799–3808, 2007. doi:10.1074/jbc.M610185200.
54. **Zakin L, De Robertis EM.** Extracellular regulation of BMP signaling. *Curr Biol* 20: R89–R92, 2010. doi:10.1016/j.cub.2009.11.021.
55. **Zhang C, McFarlane C, Lokireddy S, Bonala S, Ge X, Masuda S, Gluckman PD, Sharma M, Kambadur R.** Myostatin-deficient mice exhibit reduced insulin resistance through activating the AMP-activated protein kinase signalling pathway. *Diabetologia* 54: 1491–1501, 2011. doi:10.1007/s00125-011-2079-7.
56. **Zhao B, Wall RJ, Yang J.** Transgenic expression of myostatin propeptide prevents diet-induced obesity and insulin resistance. *Biochem Biophys Res Commun* 337: 248–255, 2005. doi:10.1016/j.bbrc.2005.09.044.
57. **Zhu X, Topouzis S, Liang LF, Stotish RL.** Myostatin signaling through Smad2, Smad3 and Smad4 is regulated by the inhibitory Smad7 by a negative feedback mechanism. *Cytokine* 26: 262–272, 2004. doi:10.1016/j.cyto.2004.03.007.